Cite this article as: Narayan Sundaram, T.N.Farris and S. Chandrasekar: JKR adhesion in cylindrical contacts. *Journal of the Mechanics and Physics of Solids.* doi:10.1016/j.jmps.2011.10.002

JKR Adhesion in Cylindrical Contacts

Narayan Sundaram [a,*] T.N. Farris [b] S. Chandrasekar [a]

[a] *Center for Materials Processing and Tribology, Purdue University, 315 N. Grant Street., West Lafayette, IN 47907-2023, USA*

[b] *School of Engineering, Rutgers, The State University of New Jersey, 98 Brett Rd., Piscataway, NJ 08854-8058, USA*

Abstract

Planar JKR adhesive solutions use the half-plane assumption and do not permit calculation of indenter approach or visualization of adhesive force-displacement curves unless the contact is periodic. By considering a conforming cylindrical contact and using an arc crack analogy, we obtain closed-form indenter approach and load-contact size relations for a planar adhesive problem. The contact pressure distribution is also obtained in closed-form. The solutions reduce to known cases in both the adhesion-free and small-contact solution (Barquins, 1988) limits. The cylindrical system shows two distinct regimes of adhesive behavior; in particular, contact sizes exceeding the critical (maximum) size seen in adhesionless contacts are possible. The effects of contact confinement on adhesive behavior are investigated. Some special cases are considered, including contact with an initial neat-fit and the detachment of a rubbery cylinder from a rigid cradle. A comparison of the cylindrical solution with the half-plane adhesive solution is carried out, and it indicates that the latter typically underestimates the adherence force. The cylindrical adhesive system is novel in that it possesses stable contact states that may not be attained even on applying an infinite load in the absence of adhesion.

Key words: Adhesion, JKR, Cylinder, Conforming, Analytical Solution

* Corresponding author.
Email address: n0000000@purdue.edu (Narayan Sundaram).

1 Introduction

The phenomenon of adhesion was first addressed in the context of elastic contacts by Johnson, Kendall and Roberts (1971) in their eponymous JKR theory, which treated the adhesive contact of two spheres. The pressure distribution for adhesive sphere contacts was shown to consist of a bounded component and an unbounded tensile component, with the latter representing unloading from a fictitious, bounded-pressure state. The unloading was proved to be equivalent to indentation of a half-space by a flat-punch with tensile resultant load. The superposed pressure traction is tensile and unbounded at the ends; the equilibrium contact size is obtained from energy considerations. Maugis and Barquins (1978) placed the JKR theory in a stronger theoretical framework of linear elastic fracture mechanics and thermodynamics. After noting that Sneddon's work on axisymmetric contact problems could be used to solve *any* adhesive axisymmetric contact problem, i.e. not just spheres, Maugis (2000) made the astute observation that the JKR theory lies entirely within the classical theory of elasticity.

JKR-type analyses have been developed for many different types of contacts. JKR adhesion has been applied to viscoelastic adhesive spherical contacts by Haiat et al (2003). There is also substantial work of this type in the membrane literature. In planar contacts, Barquins (1988) and Chaudhary and Weaver (1996) considered the important case of half-plane cylinder contacts with adhesion. Subsequently, Johnson (1995) treated the periodic or wavy adhesive contact problem. Axisymmetric and unsymmetric versions of this problem were considered respectively by Guduru (2007) and Carbone and Mangialardi (2004), the former in the single contact regime.

Most of these developments, in particular the planar adhesive contact solutions listed above, rely on the use of the half-plane approximation. However, use of the half-plane model is intrinsically limited in that the approach of the bodies cannot be calculated in general unless the contact is periodic. [1] This is due to the unboundedness of the elastic displacements at infinity in the half-plane model. As a consequence, one typically never sees the complete set of equilibrium curves for planar contacts with adhesion. This deficiency is overcome in the present work by taking into consideration the exact geometry of the contacting bodies, i.e. by considering a cylindrical, conforming contact system. Notably, this system is one of the few planar contact geometries for which closed-form approach calculations are possible.

An equally important motivation for exploring the cylindrical system is the recent interest in shape effects in adhesive contacts (Kendall et al, 2011). For instance, it has been shown how to design with multiple contacts may enhance the effect of adhesion in patterned surfaces (Spolenak et al, 2005). Design with surfaces of matching (conforming) curvatures seems like another possible way to accentuate adhesive effects.

[1] See Carbone and Mangialardi (2008). However, the load transmitted across the periodic contact is infinite.

The Barquins half-plane solution is inapplicable to describe the adhesive behavior of such systems, and a more exact description of the geometry required.

The methods used to obtain JKR adhesive solutions in the literature also deserve comment. The solution is typically presented as the superposition of a known, bounded contact solution and (unbounded) punch or crack solution. A superficial reading of the literature holds considerable risks for those wishing to obtain such solutions for other geometries, since this *ad hoc* procedure obscures the primacy of the contact boundary conditions. For instance, in the conforming cylindrical contacts considered in the present work, there is no obvious punch or independent crack solution to be added to the bounded contact solution to produce the JKR result. The existence of a handy punch solution is a consequence of regarding the contacting bodies as half-planes (two-dimensions) or half-spaces (three-dimensions), a conclusion that may be arrived at by examining the arguments used to justify the punch analogy (Johnson, 1958).

It is worth emphasizing that the JKR adhesive problem is essentially a contact mechanics problem. Consequently, there is a close connection between the JKR adhesive and non-adhesive contact problems for smooth profiles. The boundary conditions for the former are the same as those of its non-adhesive counterpart, with the difference that the condition for boundedness of pressure at the ends of the contact is relaxed and replaced by the Griffith energy release-rate condition to determine the equilibrium contact size. For physical validity, this choice must also lead to tensile singularities at the contact ends.[2] Since the boundedness of the contact pressure is a necessary condition for the contact inequalities to be satisfied (Barber, 2010), it is clear that the unbounded solution must violate one or both of the contact inequalities. For the purposes of JKR adhesion, one is interested in such solutions in which the unilateral gap inequality $gap \geq 0$ continues to hold, but the pressure is no longer unilateral i.e. the inequality $pressure > 0$ is relaxed inside the contact. This fact can only be checked by computing the gap function *a posteriori*, but such a step is essential to ensure the correctness of the purported JKR solution.

The objectives of the present work are to build a JKR model for planar contacts in which the approach can be calculated in closed-form. This is done by considering conforming cylindrical geometry and solving the unbounded pressure, JKR adhesive contact problem for this case. It thus becomes possible to provide load-approach and other equilibrium curves for cylindrical contacts. In addition, the chosen geometry illustrates the effects of confinement on adhesion, the accuracy of the Barquins half-plane adhesive approximation and the importance of enforcing the unilateral gap inequality in adhesive contacts.
This paper is organized as follows. The governing equations for the cylindrical adhe-

[2] For instance, it is possible to construct unphysical solutions with compressive singularities to adhesive contact problems, but a simple calculation reveals that the gap inequality is violated outside the contact in such cases.

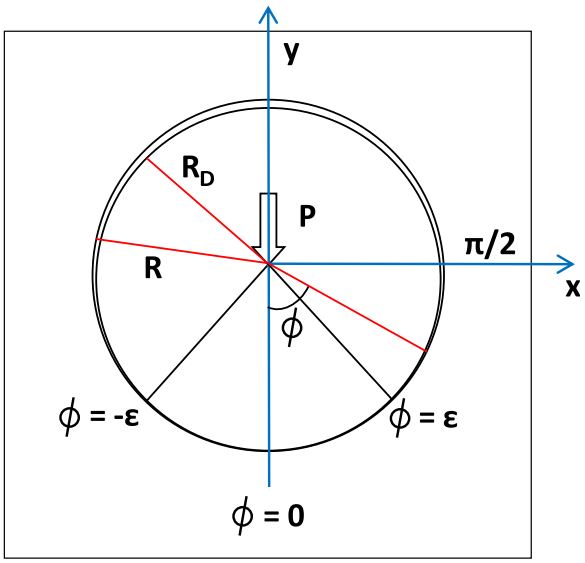

Fig. 1. Cylindrical contact geometry. The cylinder and the confining body are assumed to be in contact at a single point at $\phi = 0$ in the reference state.

sive contact problem are formulated and solved in section 2. Using a stress-intensity calculation (section 3), closed-form load/contact-size and approach/contact-size relations are obtained in sections 4 and 5. Equilibrium curves and pressure tractions of the cylindrical adhesive system are plotted in section 6. Known limiting solutions and numerous special cases, including the detachment of a rubbery cylinder from a rigid cradle, are considered in section 7. Finally, some implications of the findings of the present work, including comparison with the Barquins half-plane solution, are discussed in section 8. It is assumed that the contact is frictionless. For reasons of analytical feasibility, Dundurs' second parameter will be set to zero.

2 Formulation and solution of governing equations

The equation governing frictionless cylindrical contacts (see Fig. 1) without adhesion is a singular integro-differential equation (Ciavarella and Decuzzi, 2001). This form of the equation is valid when the pressure $N(\psi)$ is bounded and vanishes at the ends of contact; in the more general case[3] when the pressure is possibly unbounded with an integrable singularity at the ends, it may be shown using appropriate Green's functions (Sundaram and Farris, 2010) that the contact pressure obeys the following hypersingular integral equation

[3] At least in the case $\alpha^* = 0$, it is straightforward to demonstrate that the SIDE does not have unbounded solutions; in this instance, the SIDE degenerates into an SIE for $N'(\phi)$, whose solution has at most end-point singularities of strength 1/2. On integration, this yields bounded $N(\phi)$.

$$R_D - R = \frac{R}{4\pi}\left[\frac{\kappa+1}{2G}\int_{-\epsilon}^{\epsilon} N(\psi)d\psi + (\alpha^* + 2\beta^*)\int_{-\epsilon}^{\epsilon}\cos(\phi-\psi)N(\psi)d\psi \right.$$
$$\left. + \frac{\beta^*}{2}\fint_{-\epsilon}^{\epsilon}\csc^2\left(\frac{\phi-\psi}{2}\right)N(\psi)d\psi - \pi\alpha^* N(\phi)\right] \quad (2.1)$$

with the additional global equilibrium condition

$$R\int_{-\epsilon}^{\epsilon} N(\phi)\cos(\phi)d\phi = P \quad (2.2)$$

Here ϵ is the contact half-angle, and R_D and R are, respectively, the radii of the cylindrical indenter and the hole in the body containing it. The composite material parameter $\beta^* = (\kappa+1)/2G + (\kappa_I+1)/2G_I$. Like its integro-differential counterpart, Eq. (2.1) can be inverted in closed-form only when the second Dundurs' parameter $\alpha^* = 0$, i.e., when $(\kappa-1)/G = (\kappa_I-1)/G_I$. Introduce the quantity $\mathbb{B} = \int_{-\epsilon}^{\epsilon} N(\psi)d\psi$; $\mathbb{B}$ is a constant that must be obtained as part of the solution. Setting $\alpha^* = 0$, and denoting the difference in radii $R - R_D$ by Δ,

$$-\Delta = \frac{R}{4\pi}\left[\frac{\kappa+1}{2G}\mathbb{B} + 2\beta^*\int_{-\epsilon}^{\epsilon}\cos(\phi-\psi)N(\psi)d\psi + \beta^*\fint_{-\epsilon}^{\epsilon}\frac{1}{2}\csc^2\left(\frac{\phi-\psi}{2}\right)N(\psi)d\psi\right] \quad (2.3)$$

Expanding $\cos(\phi-\psi)$ as $\cos(\phi)\cos(\psi)+\sin(\phi)\sin(\phi)$, using the equilibrium relation Eq. (2.2) in Eq. (2.1) and re-arranging,

$$\left(-\Delta - \frac{R(\kappa+1)\mathbb{B}}{8\pi G}\right) - \frac{\beta^* P}{2\pi}\cos\phi = \frac{R\beta^*}{4\pi}\fint_{-\epsilon}^{\epsilon}\frac{1}{2}\csc^2\left(\frac{\phi-\psi}{2}\right)N(\psi)d\psi \quad (2.4)$$

Notice that regardless of the fact that $N(\psi)$ has singularities at the ends in the present (adhesive) case, Eq. (2.4) may be considered as a relation between two functions of ϕ. One may then *formally* integrate both sides with respect to ϕ; the constant of integration is 0 because of symmetry considerations and one obtains the following SIE

$$\left(-\Delta - R\frac{(\kappa+1)\mathbb{B}}{8\pi G}\right)\phi - \frac{\beta^* P}{2\pi}\sin\phi = -\frac{R\beta^*}{4\pi}\fint_{-\epsilon}^{\epsilon}\cot\left(\frac{\phi-\psi}{2}\right)N(\psi)d\psi \quad (2.5)$$

If one introduces the constants

$$c_0 = -\Delta - R\frac{(\kappa+1)\mathbb{B}}{8\pi G} \qquad c_1 = \frac{\beta^* P}{2\pi} \quad (2.6)$$

it is easy to show after some simple manipulations that the SIE (2.5) is a generalization of the equation for an inclusion in a plate obtained by Noble and Hussain (1969) using

completely different, dual-series summation methods and reduces to it in the special case $\Delta = 0 (R_D = R)$. In the presence of adhesion, it is more convenient to solve Eq. (2.5) by transforming it into a standard Cauchy SIE. This is done by using the change of variables $\phi = 2\tan^{-1} x$, $\psi = 2\tan^{-1} s$

$$\frac{R\beta^*}{2\pi} \int_{-a}^{a} \frac{p(s)ds}{x-s} = -2c_0 \tan^{-1}(x) + c_1 \frac{2x}{1+x^2} \tag{2.7}$$

Here $a = \tan(\epsilon/2)$ and $p(x) = N(\phi)$. The general solution to this Cauchy SIE is (Estrada and Kanwal, 2000)

$$p(x) = \frac{4}{\pi R\beta^*} \frac{1}{\sqrt{a^2-x^2}} \left[\int_{-a}^{a} \frac{\sqrt{a^2-s^2}}{x-s} \left(c_0 \tan^{-1} s - c_1 \frac{s}{1+s^2} \right) ds \right] + \frac{\mathbb{C}}{\pi\sqrt{a^2-x^2}} \tag{2.8}$$

where, by definition, the constant $\mathbb{C}$ is

$$\mathbb{C} = \int_{-a}^{a} p(x)dx \tag{2.9}$$

Note that $\mathbb{C}$, $\mathbb{B}$ and the load P are not related in a simple way. Using the integrals $I_1(x)$, $I_2(x)$ defined in the Appendix, the solution is

$$p(x) = \frac{4}{\pi R\beta^*} \frac{1}{\sqrt{a^2-x^2}} \left[c_0 I_1(x) - c_1 I_2(x) \right] + \frac{\mathbb{C}}{\pi\sqrt{a^2-x^2}} \tag{2.10}$$

Using the identity

$$\frac{1}{\sqrt{a^2-x^2}(1+x^2)} \equiv \frac{1}{\sqrt{a^2-x^2}(1+a^2)} + \frac{\sqrt{a^2-x^2}}{(1+x^2)(1+a^2)} \tag{2.11}$$

the pressure may be separated into its bounded and unbounded parts.

$$p(x) = \left[\frac{4(\sqrt{1+a^2}-1)}{R\beta^*} \left(c_0 - \frac{c_1}{\sqrt{1+a^2}} \right) + \frac{\mathbb{C}}{\pi} \right] \frac{1}{\sqrt{a^2-x^2}} + \\ + \frac{4c_1}{R\beta^*} \frac{\sqrt{a^2-x^2}}{(1+x^2)\sqrt{1+a^2}} - \frac{4c_0}{R\beta^*} \tanh^{-1} \sqrt{\frac{a^2-x^2}{1+a^2}} \tag{2.12}$$

In the transformed variables, the equations defining $\mathbb{B}$ and P may be written as

$$\int_{-a}^{a} \frac{p(x)}{1+x^2} dx = \frac{\mathbb{B}}{2} \qquad\qquad \int_{-a}^{a} p(x) \frac{1-x^2}{(1+x^2)^2} dx = \frac{P}{2R} \tag{2.13}$$

Substituting the pressure $p(x)$ from Eq. (2.12) into Eqs. (2.13),

$$r_0\int_{-a}^{a}\frac{1}{\sqrt{a^2-x^2}}\frac{dx}{(1+x^2)}+\frac{4c_1}{R\beta^*}\frac{1}{\sqrt{1+a^2}}\int_{-a}^{a}\frac{\sqrt{a^2-x^2}}{(1+x^2)^2}dx- \\ -\frac{4c_0}{R\beta^*}\int_{-a}^{a}\tanh^{-1}\left(\sqrt{\frac{a^2-x^2}{1+a^2}}\right)\frac{dx}{(1+x^2)}=\frac{\mathbb{B}}{2} \tag{2.14a}$$

$$r_0\int_{-a}^{a}\frac{dx}{\sqrt{a^2-x^2}}\frac{1-x^2}{(1+x^2)^2}+\frac{4c_1}{R\beta^*}\frac{1}{\sqrt{1+a^2}}\int_{-a}^{a}\frac{\sqrt{a^2-x^2}}{(1+x^2)}\frac{1-x^2}{(1+x^2)^2}dx- \\ -\frac{4c_0}{R\beta^*}\int_{-a}^{a}\tanh^{-1}\left(\sqrt{\frac{a^2-x^2}{1+a^2}}\right)\frac{1-x^2}{(1+x^2)^2}dx=\frac{P}{2R} \tag{2.14b}$$

where r_0 is the coefficient of the unbounded term in Eq. (2.12). Using integrals defined in the Appendix, these conditions may be written as

$$\frac{\pi r_0}{\sqrt{1+a^2}}+\frac{4c_1}{R\beta^*}\frac{\pi a^2}{2(1+a^2)}-\frac{4c_0}{R\beta^*}\frac{\pi\log(1+a^2)}{2}=\frac{\mathbb{B}}{2} \tag{2.15a}$$

$$\frac{\pi r_0}{(1+a^2)^{3/2}}+\frac{4c_1}{R\beta^*}\frac{\pi a^2(a^2+2)}{4(1+a^2)^2}-\frac{4c_0}{R\beta^*}\frac{\pi a^2}{2(1+a^2)}=\frac{P}{2R} \tag{2.15b}$$

Note that the pressure solution identically satisfies Eq. (2.9).

3 Constrained crack analogy for adhesion

The tip of the adhesive conforming contact, in keeping with the Maugis theory, is interpreted as the tip of a crack which lies exterior to the contact. Of course, unlike the straight cracks in half-plane adhesive contacts, this 'crack' is arc-shaped. In the present instance, the crack is constrained to lie along the circle $r = R$ at all times, since this is the line to which the contact boundary conditions are applied.[4] The stress-intensity factor may now be defined as follows. Consider a local coordinate system, $x' - y'$ or $\rho - \theta$, whose origin coincides with the crack-tip, with the x' axis lying along the tangent to the crack in the global coordinate system, and y' lying along the outward pointing normal. The stress intensity factor in these local coordinates is defined as

$$K_* = \lim_{\rho\to 0}\sigma_{y'y'}\sqrt{2\pi\rho} = \lim_{\rho\to 0}\sigma_{rr}\sqrt{2\pi\rho} \tag{3.1}$$

Note that the tractive state in a frictionless contact is shear-free, i.e. $\sigma_{r\theta}(\phi) = 0$. In this local coordinate system, it is easy to see that the effect of the contact traction

[4] Note that such a constraint exists in the half-plane problem as well i.e. the crack must lie on $Im(z) = 0$

is Mode-I. Furthermore, this state of affairs prevails no matter what the size of the contact.

If a point along the contact is at an angle ϕ, its angular distance from the tip of the crack is $\epsilon-\phi$ and the arc-distance is $R(\epsilon-\phi)$. This distance from the crack tip, ρ, may be re-written in terms of the 'linearized' variables, $\rho = R(2\tan^{-1}(a) - 2\tan^{-1}(x))$ to give

$$K_* = \lim_{x\to a} \sigma_{rr}\sqrt{4\pi R\left(\tan^{-1}(a) - \tan^{-1}(x)\right)} \tag{3.2a}$$

$$= \lim_{x\to a} \sigma_{rr}\sqrt{4\pi R\left(\tan^{-1}(a) - \left(\tan^{-1}(a) + \frac{x-a}{1+a^2} - \ldots\right)\right)} \tag{3.2b}$$

$$= \lim_{x\to a} \sigma_{rr}\sqrt{\frac{4\pi R}{1+a^2}}\sqrt{a-x} \tag{3.2c}$$

Here we have expanded $\tan^{-1}(x)$ about the point a, and it is easily verified that terms higher than $a-x$ may be ignored since they do not contribute to the stress-intensity factor. The presence of the $1+a^2$ factor is a consequence of the circular geometry; for small ϵ, $a = \tan(\epsilon/2)$ is very small compared to 1 and this factor has no effect on the value of K_*.

Now, since $\sigma_{rr} = -N(\phi) = -p(x)$, and the only non-zero contributions to K_* arise from singular terms in the pressure,

$$K_* = -\sqrt{\frac{4\pi R}{1+a^2}} \lim_{x\to a}\ p(x)\sqrt{a-x} \tag{3.3}$$

$$= -\sqrt{\frac{4\pi R}{1+a^2}}\sqrt{\frac{1}{2a}}\left[\frac{4(\sqrt{1+a^2}-1)}{R\beta^*}\left(c_0 - \frac{c_1}{\sqrt{1+a^2}}\right) + \frac{\mathbb{C}}{\pi}\right] \tag{3.4}$$

The virtual crack extension/closure method may now be used to relate the stress intensity factor K_* to the strain energy release rate G_*. The mode-I strain energy release rate, G_* may be written as

$$G_* = \frac{\pi}{4} A K_*^2 \tag{3.5}$$

where $A = \beta^*/2\pi$. The Griffith condition $G_* = w$ determines the contact equilibrium state, where w is the so-called Dupre energy of adhesion of the system. In terms of the stress-intensity factor, the Griffith condition is

$$\frac{\pi}{4} A K_*^2 = w \Rightarrow K_* = \sqrt{\frac{4w}{\pi A}} \tag{3.6a}$$

$$\Rightarrow \frac{4\pi}{R\beta^*}\left[\frac{(\sqrt{1+a^2}-1)}{\sqrt{1+a^2}}\left(c_0 - \frac{c_1}{\sqrt{1+a^2}}\right)\right] + \frac{\mathbb{C}}{\sqrt{1+a^2}} = -\sqrt{\frac{2aw}{AR}} \tag{3.6b}$$

It is useful to introduce the quantity $\zeta^* = \sqrt{2wR/A}$ which represents the effect of adhesive forces on the contact problem.

4 Load-contact size relation

The relations (2.15a), (2.15b) taken together with the Griffith condition Eq. (3.6) provide a system of equations that relate the contact parameter, a, to P, $\mathbb{C}$ and $\mathbb{B}$. The simplest way to proceed is to then consider a as a known quantity and solve for the latter. These equations may be written in a more compact manner as follows

$$\frac{4\pi}{R\beta^*}\Big[c_0 f_1(a) - c_1 f_2(a)\Big] + \frac{\mathbb{C}}{E} = \frac{\mathbb{B}}{2} \tag{4.1a}$$

$$\frac{4\pi}{R\beta^*}\Big[c_0 g_1(a) - c_1 g_2(a)\Big] + \frac{\mathbb{C}}{E^3} = \frac{P}{2R} \tag{4.1b}$$

$$\frac{4\pi}{R\beta^*}\Big[c_0 h_1(a) - c_1 h_2(a)\Big] + \frac{\mathbb{C}}{E} = -\frac{\zeta^*\sqrt{a}}{R} \tag{4.1c}$$

Here f_1, f_2, g_1, g_2, h_1 and h_2 consist of known rational and logarithmic functions of a, and $E = E(a) = \sqrt{1+a^2} = \sec(\epsilon/2)$.

$$f_1(a) = 1 - \frac{1}{E} - \log(E) \qquad f_2(a) = \frac{1}{E} - \frac{1}{2} - \frac{1}{2E^2} \tag{4.2a}$$

$$g_1(a) = -\frac{1}{2} + \frac{3}{2E^2} - \frac{1}{E^3} \qquad g_2(a) = -\frac{1}{4} + \frac{1}{E^3} - \frac{3}{4E^4} \tag{4.2b}$$

$$h_1(a) = 1 - \frac{1}{E} \qquad h_2(a) = \frac{1}{E} - \frac{1}{E^2} \tag{4.2c}$$

The coefficients c_0 and c_1 themselves contain $\mathbb{B}$ and P, so that upon substitution from Eq. (2.6) in Eq. (4.1) and introducing the interface parameter $\vartheta = G\beta^*/(1+\kappa)$, one finally has the following linear system

$$\begin{bmatrix} -\left(\dfrac{f_1}{2\vartheta} + \dfrac{1}{2}\right) & -\dfrac{2f_2}{R} & \dfrac{1}{E} \\ -\dfrac{g_1}{2\vartheta} & -\left(\dfrac{2g_2}{R} + \dfrac{1}{R}\right) & \dfrac{1}{E^3} \\ -\dfrac{h_1}{2\vartheta} & -\dfrac{2h_2}{R} & \dfrac{1}{E} \end{bmatrix} \begin{Bmatrix} \mathbb{B} \\ P \\ \mathbb{C} \end{Bmatrix} = \frac{4\pi\Delta}{R\beta^*} \begin{Bmatrix} f_1 \\ g_1 \\ h_1 \end{Bmatrix} - \frac{1}{R} \begin{Bmatrix} 0 \\ 0 \\ \zeta^*\sqrt{a} \end{Bmatrix} \tag{4.3}$$

This linear system is easily solved in closed-form. After simplification, the load-contact parameter $(P-a)$ relationship may be expressed as follows

$$P = \frac{2\left(1+a^2\right)\left[4\pi\Delta\dfrac{\vartheta}{\beta^*}a^2 - \zeta^*\sqrt{a}\left(a^2 - \log(1+a^2) + 2\vartheta\right)\right]}{2\vartheta - \log(1+a^2) - 2a^4} \tag{4.4}$$

Writing $L = \log(1+a^2)$, $\mathbb{B}$ and $\mathbb{C}$ are found to be

$$\mathbb{B} = \frac{4\vartheta}{R\beta^*}\frac{2\pi\Delta\left(L + 2a^4\right) - \zeta^*\beta^*\sqrt{a}\left(1+2a^2\right)}{2\vartheta - L - 2a^4} \tag{4.5a}$$

$$\mathbb{C} = \frac{8\pi\Delta\vartheta}{R\beta^*}\frac{(1-2a^2)(\sqrt{1+a^2}-1)+2a^4}{2\vartheta-L-2a^4} - \frac{\zeta^*\sqrt{a}}{R}\left(\sqrt{1+a^2}\frac{2-2a^4+3L-6\vartheta}{2\vartheta-L-2a^4} + 2\frac{4\vartheta-1-2L+2a^2(a^2-L+2\vartheta)}{2\vartheta-L-2a^4}\right) \tag{4.5b}$$

Examining Eq.(4.4), one finds that since $a^2 > \log(1+a^2)$, the quantity multiplying ζ^* is always positive. Hence, the effect of adhesion is to result in a smaller value of load P at a given value of the contact-size parameter, a, in the sub-critical range $2\vartheta - \log(1+a^2) - 2a^4 > 0$.

Further, the denominator in Eq. (4.4) goes to 0 when $2\vartheta - \log(1+a^2) - 2a^4 = 0$. The root of this transcendental equation, a_∞ or a_{crit}, is independent of both the applied load and the presence of adhesion, depending only on the composite material parameter ϑ. This is, in fact, the classical receding contact solution. For instance, when $\vartheta = 1$ (for similar materials), $a \approx 0.9135 \Rightarrow \epsilon \approx 84.823^\circ$. The $P-a$ behavior is examined more closely in later sections.

5 Calculation of the approach

It is easier to calculate the approach in the original variables. For all points inside the contact, the difference in radial surface displacements of the confining body ($\tilde{v}_r$) and the indenter ($\tilde{u}_r$) may be written as

$$\tilde{v}_r(\phi) - \tilde{u}_r(\phi) = -\Delta(1-\cos(\phi)) + \boldsymbol{\delta}\cos(\phi) \tag{5.1}$$

where $\boldsymbol{\delta}$ is the approach. Expressing $\tilde{v}_r - \tilde{u}_r$ in terms of distributed Green's functions (with $\alpha^* = 0$),

$$\boldsymbol{\delta}\cos\phi - \Delta(1-\cos\phi) = \frac{-R}{4\pi}\int_{-\epsilon}^{\epsilon} N(\psi)\left[\beta^*\boldsymbol{c}(\phi,\psi)\log(2-2\boldsymbol{c}(\phi,\psi)) + \frac{\boldsymbol{c}(\phi,\psi)}{G_I} + \frac{\kappa_I+1}{2G_I}\right]d\psi \tag{5.2}$$

where $\boldsymbol{c}(\phi,\psi) = \cos(\phi-\psi)$. Setting $\phi = 0$, using the definitions of $\mathbb{B}, P$ and changing the limits of the (even) integral to $(0,\epsilon)$

$$\boldsymbol{\delta} = -\frac{R}{4\pi}\left[\frac{\kappa_I+1}{2G_I}\mathbb{B} + \frac{P}{RG_I} + \beta^*\int_0^{\epsilon} N(\psi)\cos(\psi)4\log\left(2\sin\frac{\psi}{2}\right)d\psi\right] \tag{5.3}$$

The pressure $N(\psi)$ in the original variables is

$$N(\psi) = \frac{r_0\cos(\psi/2)\cos(\epsilon/2)}{\boldsymbol{s}(\psi,\epsilon)} + \frac{4c_1}{R\beta^*}\cos(\psi/2)\boldsymbol{s}(\psi,\epsilon) - \frac{4c_0}{R\beta^*}\log\left(\frac{\cos(\psi/2)+\boldsymbol{s}(\psi,\epsilon)}{\cos(\epsilon/2)}\right) \tag{5.4}$$

where $\boldsymbol{s}(\psi,\epsilon) = \sqrt{\cos^2(\psi/2) - \cos^2(\epsilon/2)}$ and r_0 is the coefficient of the unbounded term in Eq. (2.12). The integral(s) in Eq. (5.3) are analytically quite difficult if one considers the form of the functions appearing in $N(\psi)$; however, if the logarithmic kernel in Eq. (5.3) is expanded using the following infinite series

$$-\sum_{n=2}^{\infty} \frac{n}{n^2-1}\cos n\psi = \frac{1}{2} + \frac{\cos\psi}{4} + \cos\psi \log\left(2\sin\frac{\psi}{2}\right) \tag{5.5}$$

then it is possible to convert all the integrals involved in Eq. (5.3) either into known forms listed in Noble and Hussain (1969) or integrals derivable from them. Denote the integral in Eq. (5.3) by $J(\epsilon)$; on using the infinite series and interchanging sum and integral, one has

$$J(\epsilon) = -\mathbb{B} - \frac{P}{2R} - 4\left\{\sum_{n=2}^{\infty} \frac{n}{n^2-1}\int_0^{\epsilon} N(\psi)\cos(n\psi)d\psi\right\} \tag{5.6}$$

Substituting for the pressure $N(\psi)$,

$$J(\epsilon) = -\mathbb{B} - \frac{P}{2R} - 4\sum_{n=2}^{\infty} \frac{n}{n^2-1}\left\{\int_0^{\epsilon} \frac{r_0\cos(\psi/2)\cos(\epsilon/2)\cos(n\psi)}{\boldsymbol{s}(\psi,\epsilon)}d\psi + \right.$$
$$\left. + \frac{4c_1}{R\beta^*}\int_0^{\epsilon}\cos(\psi/2)\cos(n\psi)\boldsymbol{s}(\psi,\epsilon)d\psi - \frac{4c_0}{R\beta^*}\int_0^{\epsilon}\cos(n\psi)\log\left(\frac{\cos(\psi/2)+\boldsymbol{s}(\psi,\epsilon)}{\cos(\epsilon/2)}\right)d\psi\right\} \tag{5.7}$$

Using the sums of the infinite series of integrals listed in the Appendix, and much simplification, the approach is

$$\boldsymbol{\delta} = \frac{\mathbb{B}R}{4\pi}\frac{\kappa+1}{2G} + \frac{P}{4\pi}\left(\frac{\beta^*}{2} - \frac{1}{G_I}\right) - \left(\frac{5}{4}c_0 + c_0L_s + \frac{19}{16}c_1 + \frac{17}{8}c_1L_s\right) - \frac{c_1}{16}(5+6L_s)\cos(2\epsilon)$$
$$+ \frac{1}{4\pi}(3+4L_s)\left[4(c_0+c_1)\pi - \beta^*R\mathbb{C}\right]\cos^3(\epsilon/2) - \frac{1}{4}\left(6c_1(1+L_s) + c_0(7+12L_s)\right)\cos\epsilon \tag{5.8}$$

where $L_s = \log\sin(\epsilon/2)$. Clearly, given ϵ $(= 2\tan^{-1}(a))$, one can evaluate $\mathbb{C}$, $\mathbb{B}$ and P using Eqs. (4.4)-(4.5). With these values, $\boldsymbol{\delta}$ may be calculated with the help of Eq. (5.8) above.

Overclosure test

In the case of a confined indenter, it is essential to check that the proposed adhesive solution satisfies the gap inequality. The gap function at any location exterior to the contact is given by

$$h(\phi) = \Delta(1-\cos\phi) - \boldsymbol{\delta}\cos\phi + \tilde{v}_r(\phi) - \tilde{u}_r(\phi) \tag{5.9}$$

Under the application of a sufficiently large net upward (negative) force P, a contact will be established along the upper side of the hole. The first point of contact is invariably $\phi = \pi$ so for this purpose it is sufficient check that $h(\pi) > 0$. Expressing the surface radial displacements in terms of Green's functions and setting $\phi = \pi$,

$$h(\pi) = 2\Delta + \boldsymbol{\delta} - \frac{R}{4\pi}\left[\frac{\kappa_I + 1}{2G_I}\mathbb{B} - \frac{P}{RG_I} - \beta^* \int_0^{\epsilon} N(\psi) 4\cos\psi \log\left(2\cos\frac{\psi}{2}\right) d\psi\right] \quad (5.10)$$

In this case, the integral $J_\pi(\epsilon)$ appearing in Eq. (5.10) may be expressed as the sum of infinite series of Legendre polynomials using the Mehler integral formula; however, since $N(\phi)$ is known in closed-form, it is far more convenient to use adaptive Gauss-Kronrod quadrature for computational purposes. Candidate adhesive solutions with $h(\pi) < 0$ are unacceptable. This technique may also be used to obtain the gap at an arbitrary location (i.e. other than $\phi = \pi$) and ensure that the solution satisifies $h(\phi) > 0$ at all locations exterior to the contact.

6 Equilibrium curves for cylindrical adhesive contacts

The relations (4.4) and (5.8) make it possible to draw the equilibrium curves of the adhesive contact system; Eq. (5.10) and gap calculations elsewhere allow one to check whether the JKR solution satisfies the (essential) gap inequality. The more general case of non-zero clearance $\Delta > 0$ and finite ϑ is examined first. Special cases are considered separately. For this purpose, it is helpful to introduce the normalized adhesion strength $M = \sqrt{wAR}/(\sqrt{2}\Delta\vartheta)$ and normalized load $P^* = P\beta^*/(4\pi\Delta\vartheta)$.

An examination of Eq. (4.4) reveals that the critical contact parameter a_{crit} demarcates two distinct regimes of adhesive contact behavior, namely the sub-critical regime ($a < a_{crit}$) and super-critical ($a > a_{crit}$) regime. Since a has no upper-bound in the super-critical regime, it is more convenient to use the normalized contact half-angle $\epsilon^* = 2\tan^{-1}(a/a_{crit})/\pi$. Note that the contact parameter a, and the contact half-angle ϵ are related by $\epsilon = 2\tan^{-1} a$. The positive direction for the load P^* and approach $\boldsymbol{\delta}$ is downward; upward loads / approach are considered negative.

Sub-critical equilibrium curves for $\vartheta = 1$ at various values of M are shown in Fig. 2, with the adhesionless case also indicated for reference. Plot 2d is not an equilibrium curve, but the result of the overclosure calculation. The dashed lines in all plots indicate equilibria that violate the gap inequality (inadmissible states). In plot 2a, one sees that at lower values of M, a non-trivial zero-load equilibrium exists in addition to the $(0, 0)$ state, which implies that JKR 'snap-in' occurs. Similarly, the presence of tensile P^* minima for these values of M indicates classical fixed-load separation behavior at a non-zero contact size. For net downward loads, the normalized contact parameter a/a_{crit} increases asymptotically to 1 as $P^* \to \infty$, which is characteristic of cylindrical contacts.

At higher values of M, there is a qualitative change in this behavior. The tensile minima in the $P^* - a^*$ curves disappear and the cylinder is essentially confined, i.e. larger and larger upward forces P^* are supported till overclosures occur at $\phi = \pi$. In such a case, the equilibrium must be sought over two separate (in general, unequal) contact patches. Neither the pressure nor the $P-a$ relation may be determined in closed-form in this regime. Plot 2b shows that the contact parameter / approach behavior is very similar. The load-approach equilibrium plot 2c shows that at lower values of M, the equilibrium curves contain a full loop with minima in both P^* and approach δ/Δ. At higher values of M, the curves 'unfold' and the P^* minima disappear; a more negative (upward) load causes sufficiently large upward displacement to result in overclosures near $\phi = \pi$.

Plots 3a and 3b show a close-up of the equilibrium curves for the lower range of M values. The minima indicated with the letter 'x' are the adherence forces (or lift-off forces) at fixed load at the indicated values of M. The minima indicated with the circles are the adherence forces at fixed grips. A more detailed discussion of fixed-load stability is provided in a later section.

If one now examines the pressure tractions at representative load points at some value of M (Fig. 4), the interplay between the bounded and unbounded components of pressure (due to adhesion) is clearly seen. At a highly compressive load $P^* = 4.0$, the pressure traction is compressive (positive) along most of the contact, with narrow tensile patches existing only near the edges of contact. At lower values of P^*, these patches of negative pressure extend further and further into the central compressive region. Finally, at a point close to detachment, it is possible for the pressure traction to be entirely tensile ($P^* = -0.15$, Fig. 4d). This behavior (at sub-critical a) is qualitatively quite similar to that seen in classical JKR contacts (Maugis, 2000).

The existence of super-critical equilibria is a novel feature of adhesive conforming contacts. The contact arc sizes in this regime are greater than the largest possible arc size (attained upon application of an infinite load) in the absence of adhesion. One sees in plot 5a that for some intermediate values of the adhesion parameter (e.g. $M = 0.4$) fixed-load detachment occurs at some super-critical contact angle/contact parameter. As M is increased further, this value shifts and becomes less negative; it ceases to be a 'detachment' load once the minimum of the $\epsilon^* - P^*$ curve shifts into the region of positive P^*. For large values of M, only supercritical equilibria exist for highly positive P^*. The apparent anomaly of the lack of non-trivial equilibria at high M and 0 load (indeed, for moderately positive loads) is explained in section 8.

Lastly, if one uses a material pair with a different value of ϑ (0.5, corresponding to a rigid cylindrical indenter), one sees from Fig. 6 that the equilibrium curves look qualitatively similar to the case $\vartheta = 1.0$. However, in this instance, the value of M at which the system transitions from the regime of 'detachment' to 'no-detachment' is higher. Again, the dashed lines indicate infeasible or gap-violating solutions.

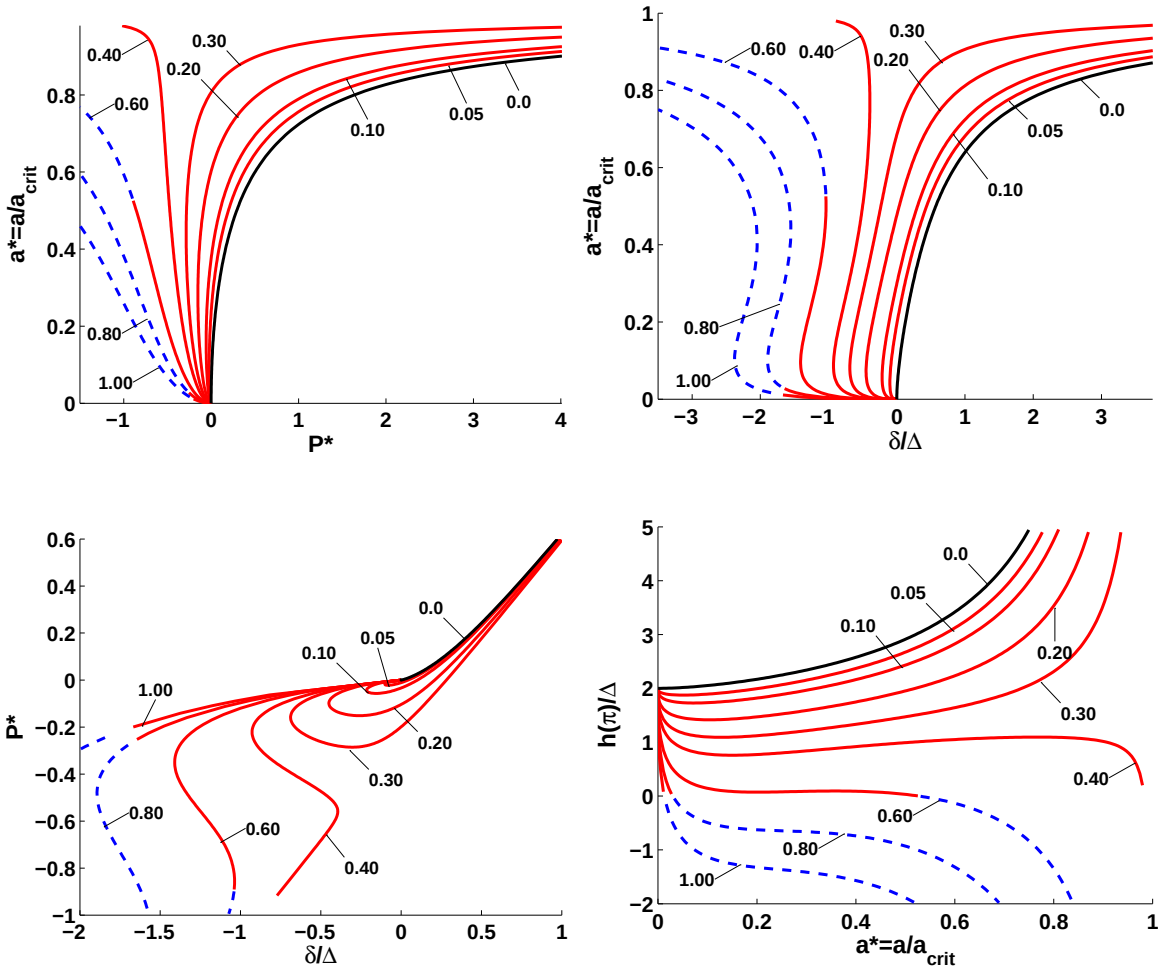

(c) (d)

Fig. 2. Equilibrium curves in the sub-critical region $a < a_{crit}$ for $\vartheta = 1.0$. The normalized adhesion parameter M varies from 0 to 1 and is indicated on the plots.

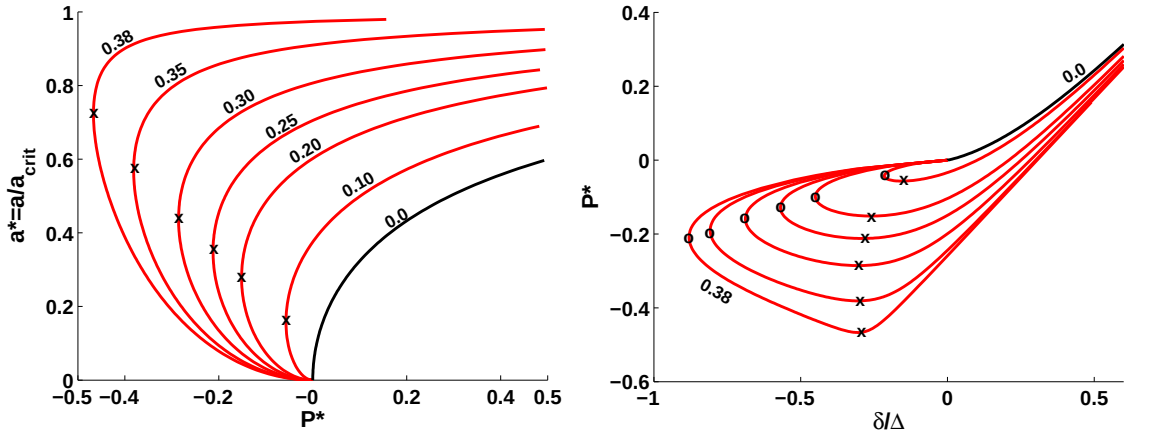

(a) (b)

Fig. 3. Plot (a) is a close-up of the adhesive $P^* - a^*$ plot with detachment loads indicated with an x. Plot(b) is a close-up of the $\delta/\Delta - P^*$ plot with detachment loads indicated.

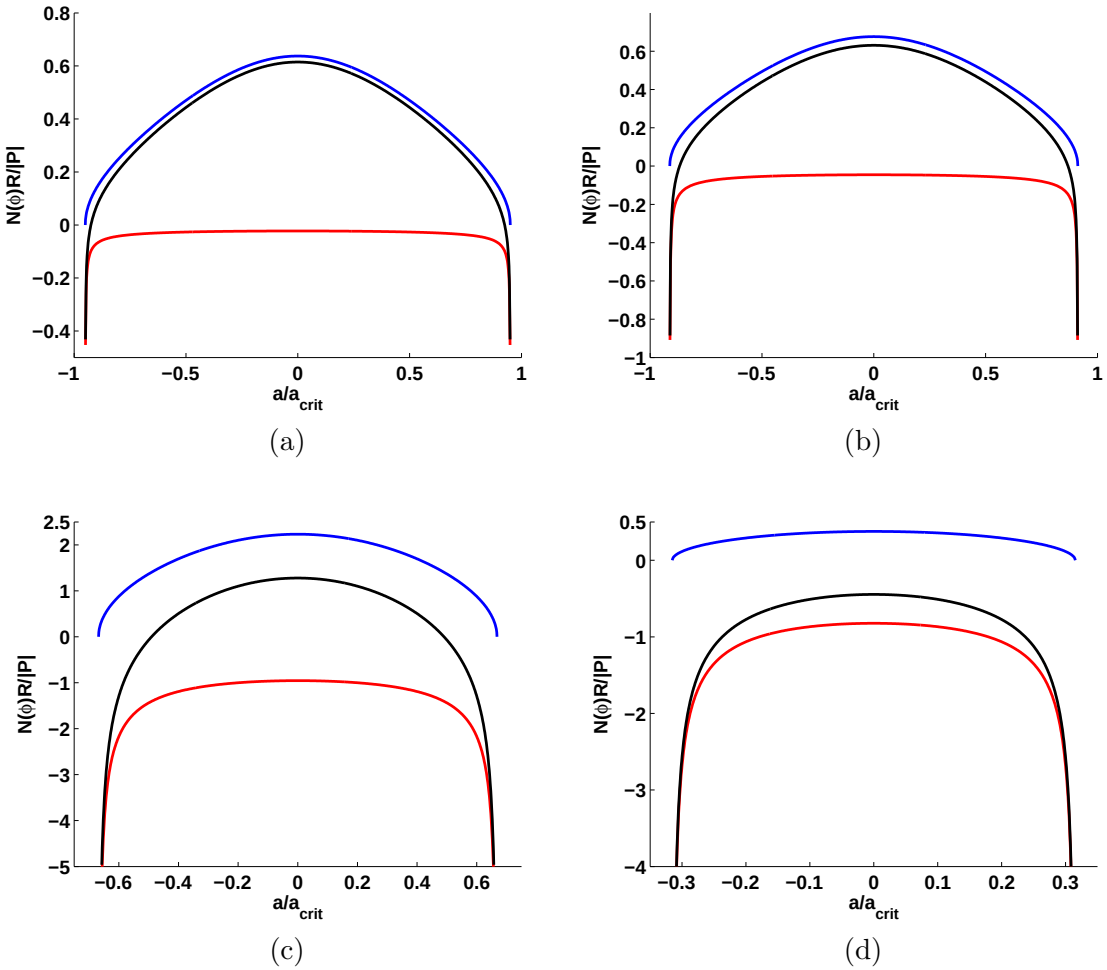

Fig. 4. Bounded, unbounded(tensile) and total components of the normalized contact pressure traction $N(\phi)R/|P|$ at $M = 0.2$ and $P^* = 4$, $P^* = 2$, $P^* = 0.1$ and $P^* = -0.15$ in the sub-critical region $a < a_{crit}$. $\vartheta = 1.0$.

7 Reduction in special cases

When there is no adhesion, $\zeta^* = 0$, and the load-contact parameter Eq. (4.4) reduces to the following (known) standard form on re-substituting $G\beta^*/(1+\kappa)$ for ϑ

$$P|_{w=0} = \frac{8\pi\Delta G a^2\,(1+a^2)}{2G\beta^* - (L+2a^4)(1+\kappa)} \tag{7.1}$$

Further $\mathbb{B}R/P$ reduces to the following standard form

$$\left.\frac{\mathbb{B}R}{P}\right|_{w=0} = \frac{\log(1+a^2)+2a^4}{a^2(1+a^2)} \tag{7.2}$$

As $a \to 0$, it is easily verified that $\mathbb{B}R/P \to 1$ in the above equation.

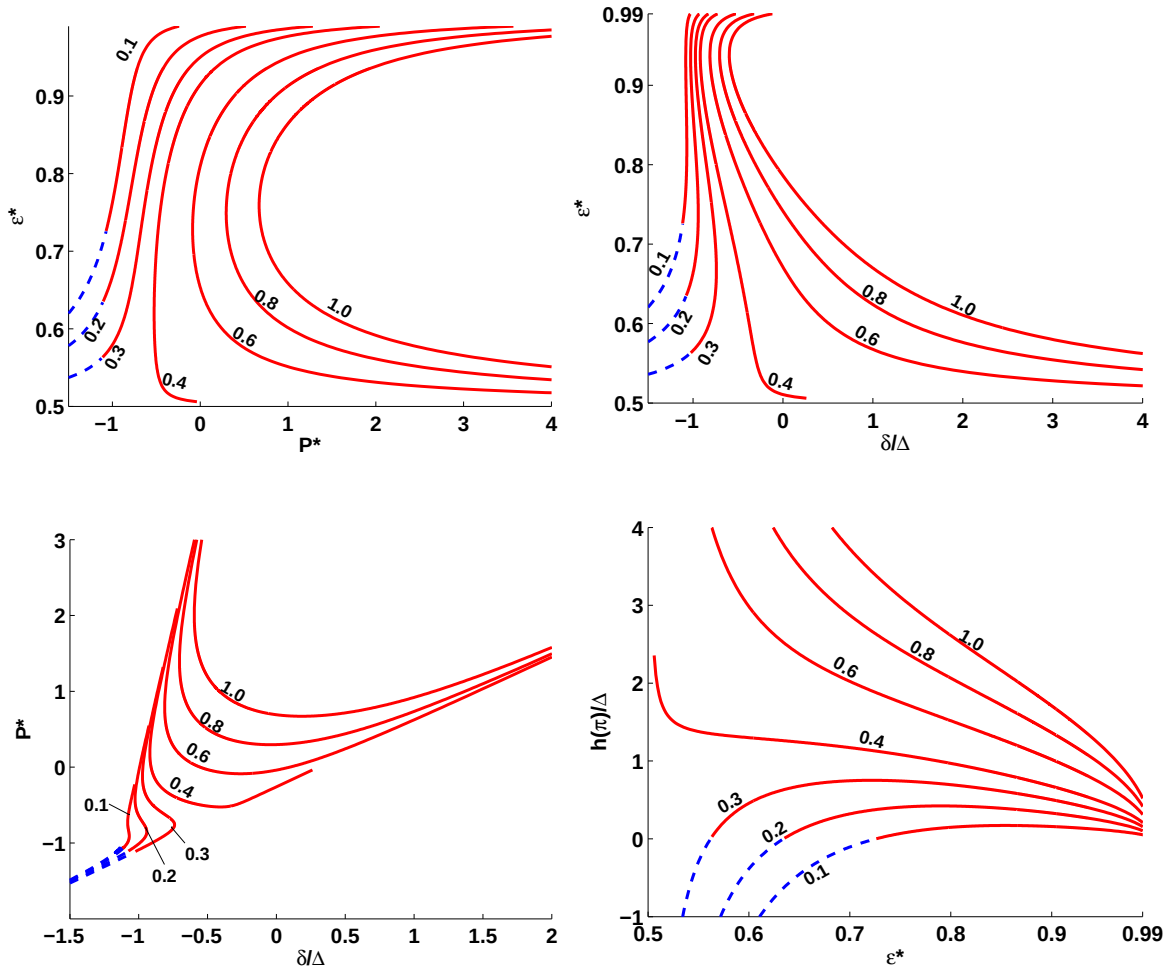

(c) (d)

Fig. 5. Equilibrium curves in the super-critical region $a > a_{crit}$ for $\vartheta = 1.0$. The normalized adhesion parameter M varies from 0 to 1 and is indicated on the plots.

7.1 Reduction to Barquins' solution at small contact size

An important test of conforming contact solutions is that they must reduce (under suitable assumptions) to their half-plane counterparts. In the present instance, it must be possible to recover the Barquins (1988) non-conforming adhesive contact solution for small a. Using the series expansion $L = \log(1+a^2) = a^2 - a^4/2\ldots$ in Eq. (4.4)

$$P_h = \frac{2\,(1+a^2)\left[4\pi\Delta\dfrac{\vartheta}{\beta^*}a^2 - \zeta^*\sqrt{a}\,(2\vartheta + (a^2 - (a^2 - a^4/2\ldots)))\right]}{2\vartheta - (a^2 - a^4/2\ldots + 2a^4)} \tag{7.3a}$$

$$\Rightarrow P_h\beta^* \approx \frac{2\beta^*}{2\vartheta}\left[4\pi\Delta\frac{\vartheta}{\beta^*}a^2 - \sqrt{a}\zeta^* 2\vartheta\right] \tag{7.3b}$$

$$\Rightarrow P_h\beta^* \approx 4\pi(R - R_D)a^2 - 2\beta^*\sqrt{a}\sqrt{\frac{2wR}{A}} \tag{7.3c}$$

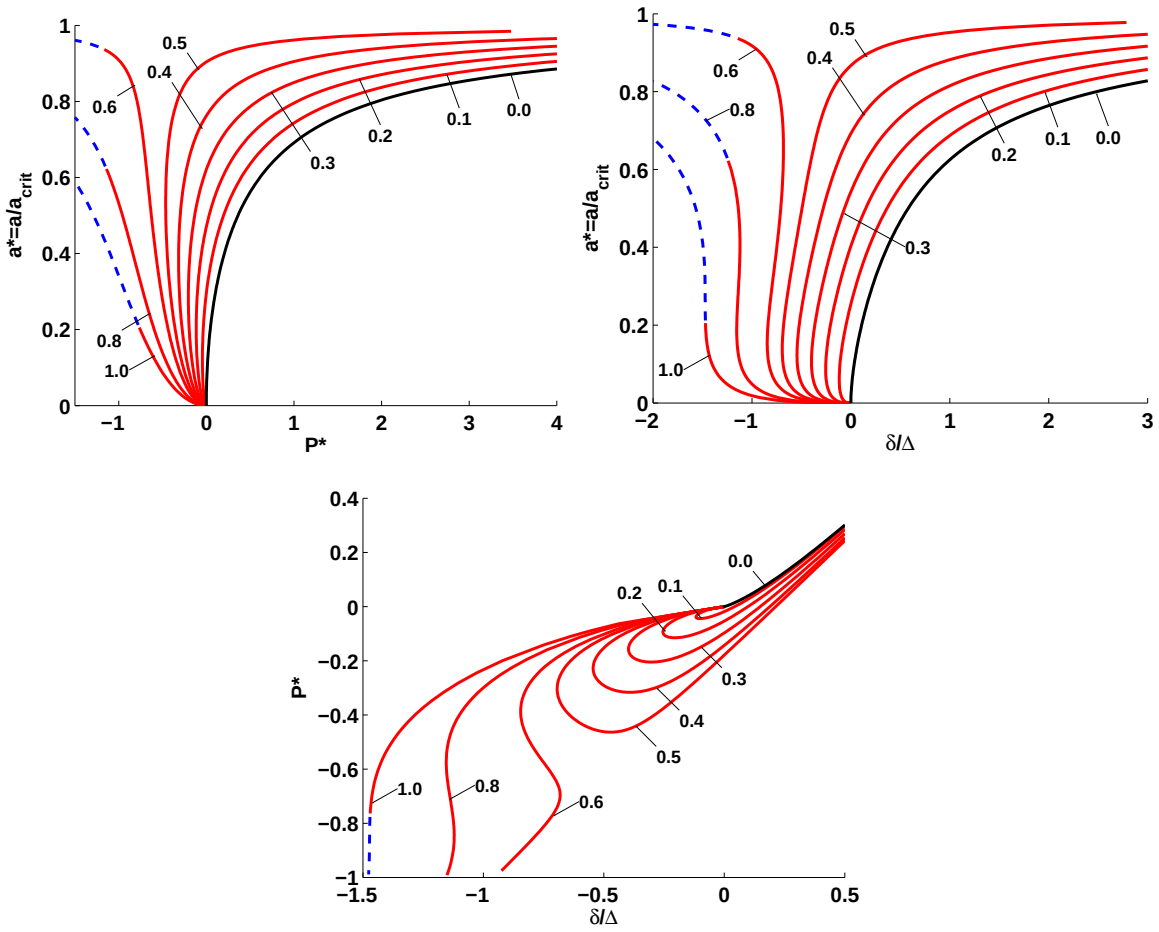

(c)

Fig. 6. Equilibrium curves in the sub-critical region $a < a_{crit}$ for $\vartheta = 0.5$. The normalized adhesion parameter M varies from 0 to 1 and is indicated on the plots.

The simplification from Eq. (7.3a) to Eq. (7.3b) is based on the fact that $1 + a^2 \approx 1$ and $a^2 << 2\vartheta$ for small a. Since the contact half size, $R\epsilon = 2R\tan^{-1}(a) \approx 2aR$ it is convenient to introduce the contact length $a_h = 2aR$. Using the relation $\beta^* = 2\pi A$, introducing the composite curvature $1/R^* = 1/R_D - 1/R$ and re-arranging, one has

$$P_h = \frac{a_h^2}{2AR^*}\frac{R_D}{R} - \sqrt{\frac{4a_h w}{A}} \tag{7.4}$$

If one considers that $R_D \approx R$ in the conforming contact formulation, this result is essentially the same as that obtained by Barquins (1988) and Chaudhary and Weaver (1996) for adhesive contacts using the half-plane assumption. Further, when $w = 0$, one recovers the Hertz load-contact size relation for cylinders.

7.2 Detachment of a rubbery cylinder from a stiff cradle

Consider a rubbery cylinder ($\nu_I \approx 0.5 \Rightarrow \kappa_I \approx 1$) of radius R_D resting on a rigid, circular cradle of slightly larger radius R. In this instance, the $P-a$ relation simplifies considerably. In fact, the adhesive behavior is also qualitatively different. Letting $\vartheta \to \infty$ in Eq. (4.4),

$$P = 4\pi(1+a^2)\Delta\frac{a^2}{\beta^*} - 2(1+a^2)\sqrt{\frac{2waR}{A}} \tag{7.5}$$

which, on introducing the non-dimensionalized variables $P_R^* = P\beta^*/(4\pi\Delta)$, $M_R^* = \sqrt{wAR}/\sqrt{2}\Delta$ has the simple form

$$P_R^* = (1+a^2)\left[a^2 - 2M_R^*\sqrt{a}\right] \tag{7.6}$$

This equation always has a non-trivial ($a > 0$) solution for the equation $P_R^* = 0$ as well as any positive load. Further, it is seen that the predicted normalized load exceeds the half-plane / Barquins solution by a factor of $1+a^2$. Setting $dP^*/da = 0$, the contact parameter at lift-off is given by the following non-linear equation

$$4a^{7/2} - 5M_R^*a^2 + 2a^{3/2} - M_R^* = 0 \tag{7.7}$$

Since the critical contact parameter $a_{crit} \to \infty$ as $\vartheta \to \infty$, no super-critical equilibrium states exist. Further, there is always a lift-off / adherence force at fixed load for every given value of M_R^*. However, the effect of the confinement manifests itself in gap violations at large M_R^* and sufficiently negative $\boldsymbol{\delta}$. Fig. 7 shows the equilibrium curves for separation of a rubbery cylinder from a closely conforming rigid cradle by forces distributed uniformly over its interior. Note that the a^*-P^* curves do not have asymptotes since a_{crit} lies at ∞, and in this respect the $\vartheta = \infty$ case is qualitatively most similar to the half-plane adhesive solution.

7.3 Neat-fit adhesive behavior

Another special case of adhesive behavior is that of the initial neat-fit ($\Delta = 0$). An examination of Eq. (4.4) reveals that the denominator goes to 0 when $2\vartheta - \log(1+a^2) - 2a^4 = 0$. In the adhesion-free case, this corresponds to the solution at infinite P as well as neat-fit. The key difference when adhesion is present is that these two cases are no longer identical. For infinite load the presence of adhesion has no effect on the contact size, which depends only on the interface parameter ϑ as mentioned in section 4. For the neat-fit, the numerator is strictly negative, and a necessary condition for Eq. (4.4) to be satisfied for positive P is for the denominator to also assume a negative value, so that in this case $a \neq a_{crit}$. Further, since $2\vartheta - \log(1+a^2) - 2a^4$ is a decreasing function of a, one infers that $a_{\Delta=0} > a_\infty$, or, $\epsilon_{\Delta=0} > \epsilon_\infty$. Consequently the contact

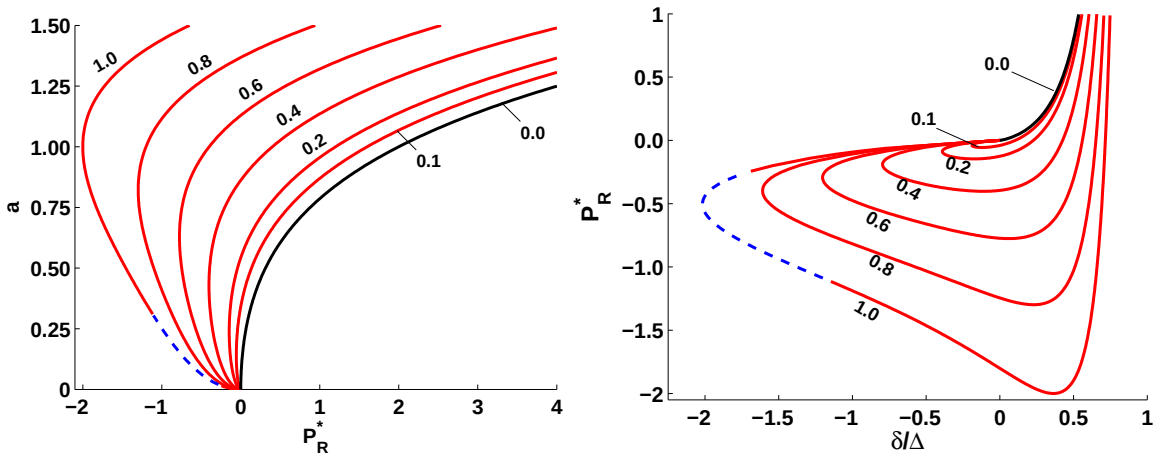

(a) (b)

Fig. 7. Equilibrium curves for a rubbery cylinder on a rigid cradle ($\vartheta = \infty$). All the equilibria are sub-critical.

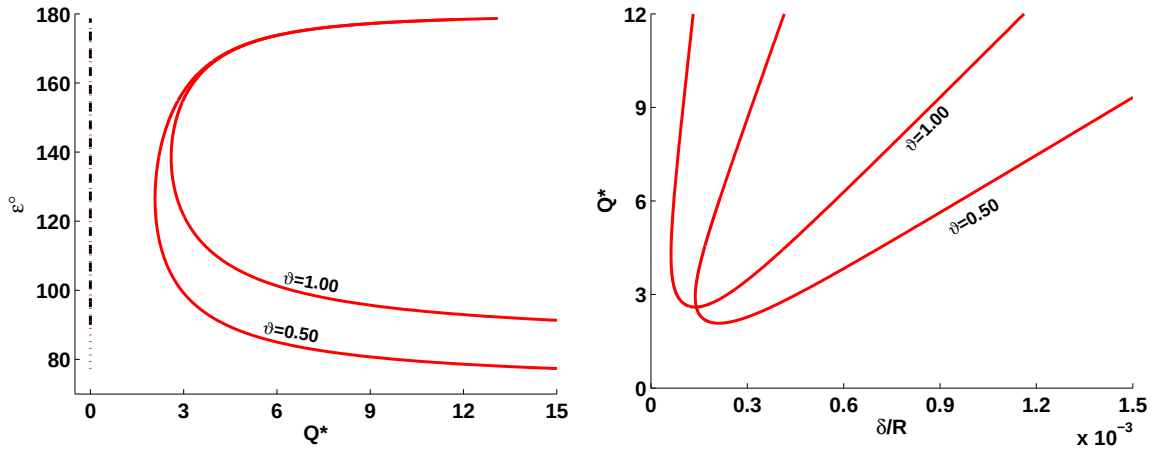

(a) (b)

Fig. 8. Equilibrium curves for neatfit ($\Delta = 0$). Only super-critical equilibria satisfy $h(\phi) > 0$. The curves are at $\vartheta = 0.5$ and $\vartheta = 1.0$. When the combined load/adhesion parameter $Q^* = \infty$ (no adhesion or infinite load), the contact angle is the critical angle.

angle with neat-fit adhesion at any downward load is 1) Strictly greater than the infinite-load angle and 2) No longer independent of the applied load P.

In the adhesionless neat-fit problem, it is well known (Gladwell, 1980) that the cylinder separates on application of the slightest downward force P. In the presence of adhesion, a non-zero downward load has to be applied to overcome the adhesive attraction between the cylinder and the conforming surface to achieve separation. This effect is demonstrated by the load-contact angle curves in Fig. 8a. The combined load parameter is defined as $Q^* = P\sqrt{A}/\sqrt{2wR}$. When w is small, Q^* is very large and separation (i.e. to any point on the equilibrium curve) occurs easily. For larger values of w (smaller Q^*) the separation loads become even higher. Finally, beyond some threshold value of w, separation only occurs at an infinite value of P.

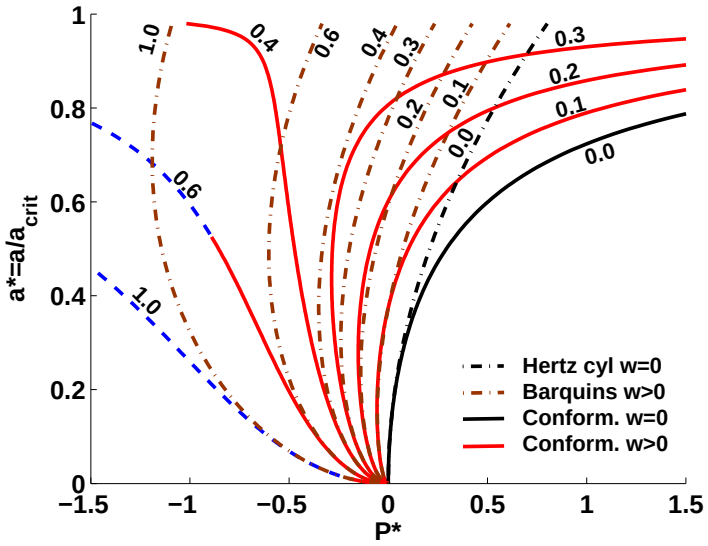

Fig. 9. A comparison of equilibrium $a^* - P^*$ curves at $\vartheta = 1.0$. The Barquins half-plane solution ($M > 0$), Hertz half-plane solution ($M = 0$), non-adhesive cylindrical solution ($M = 0$) and adhesive cylindrical solution $M > 0$ are plotted.

8 Discussion

The findings in this paper may be grouped and used in one of the following three ways: 1) In the sub-critical regime, one may use the results to obtain the indenter approach for cylindrical adhesive contacts in closed-form and get better estimates of the $P^* - a^*$ / detachment behavior over the Barquins half-plane adhesive calculation. 2) Separately, if one considers the contact as confined, the results demonstrate the influence of the confining geometry on adhesive contact behavior in both sub- and super-critical regimes. 3) The findings shed light on the limitations of methods typically used to obtain JKR type solutions to other contact systems. Each of these aspects is now considered in turn.

8.1 Comparison with the Barquins half-plane adhesive model

As shown in Sec. 7.1, the adhesive contact solution in the present work reduces to the half-plane adhesive solution in the limit of small a. A comparison of the equilibrium subcritical $P^* - a^*$ curves is shown in Fig. 9. One sees that the half-plane solution predicts a minimum P^* at all M, and it cannot model the confinement effect, which leads to overclosures. As expected, both models agree closely when a is small. The accuracy of the half-plane model depends not only on the contact-size, but also on the strength of the adhesion M. It may be noted that the deviation is worse at higher values of M.

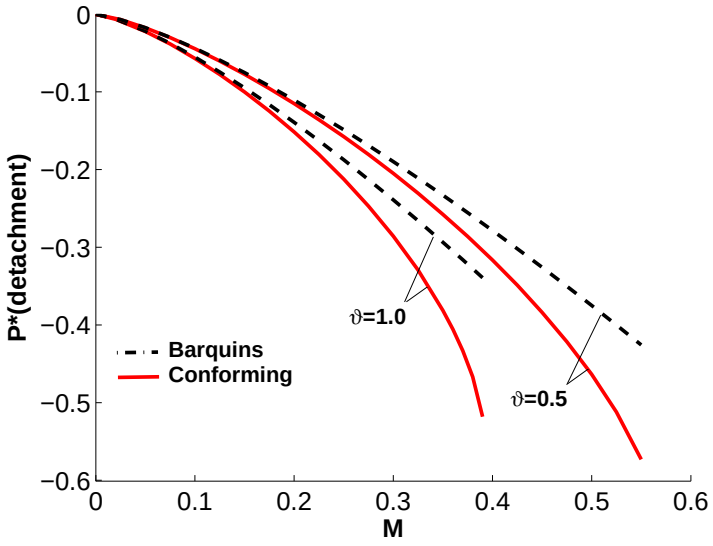

Fig. 10. A comparison of conforming cylinder and Barquins detachment loads as a function of M at $\vartheta = 0.5$ and $\vartheta = 1.0$.

On comparing the predicted normalized lift-off forces P^* according to both models in the regime where the conforming contact shows constant-load detachment (Fig. 10), it is seen that the half-plane adhesive solution consistently under predicts the value of the adherence force. This is a consequence of the conforming geometry and is not unexpected.

8.2 Highly adhesive contacts and super-critical equilibria

As mentioned in section 6, for large values of the adhesion parameter M, two kinds of apparently anomalous phenomena occur. The first involves the lack of a minimum in the $P^* - a^*$ sub-critical equilibria for sufficiently large M. At first glance, this seems to imply that an arbitrarily high upward (negative) load P^* may be sustained by the contact before detachment. However, if one considers the gap overclosure test, one sees that such equilibria (dashed lines in plot 2a) are infeasible and a second contact is invariably established at a large but finite value of this load, thus preventing the physically unexpected, infinite detachment load.

The second such manifestation is more subtle, and it may be seen by examining the contact parameter at zero load. Writing $M = \sqrt{wAR}/(\sqrt{2}\Delta\vartheta)$ in Eq.(4.4), and eliminating the trivial root $a = 0$, the zero-load contact parameter, a_0, is obtained by solving the following transcendental equation

$$\frac{1}{M}a_0^{3/2} - a_0^2 - 2\vartheta + \log(1 + a_0^2) = 0 \tag{8.1}$$

This equation must be solved numerically for a_0; however, for $a_0 < 1$, an excellent

approximation may be obtained by expanding $\log(1+a^2)$, which gives $a_0 \approx (2\vartheta M)^{2/3}$ i.e. $a_0 \approx (2wAR)^{1/3}\Delta^{-2/3}$. Thus, as expected, one sees non-zero contact sizes even at 0 load and a consequent JKR type snap-in from the trivial equilibrium $a = 0$ to a_0.

However, the dominance of the a_0^2 term in Eq. (8.1) for large a_0 leads to an interesting consequence: Eq. (8.1) does not have a solution for sufficiently large values of M (i.e. large w). This means that for sufficiently large M and no applied load, only the trivial equilibrium $a = 0$ exists.

Further, for even larger values of M and weakly positive loads P^*, the Griffith condition $G = w$ cannot be satisfied and there is no static solution to the adhesive problem. The zero-load and weakly-positive load anomalies may be explained by the fact that adhesion in the cylindrical system involves two separate effects, which begin to oppose rather than complement each other as a increases. Consider the simpler case of $P^* = 0$: In the sub-critical range, the adhesive forces have a tendency to increase the size of the contact, i.e. they lead to a larger value of a_0 and hence ϵ_0. If the value of adhesion is large enough, sub-critical a_0 may be inadequate to allow sufficient expansion of the contact. This may be overcome at moderately large values of M by allowing supercritical contact sizes up to $a_0 = 1(\epsilon = \pi/2)$. However, this process cannot be sustained at even larger values of M because the contribution of the tensile edge pressures to the resultant P, unlike half-plane contacts, is not unidirectional. For contact half-angles ϵ much beyond $\pi/2$, this contribution changes direction from upwards to downwards, and can only be in equilibrium with a minimum positive P (non-zero P). This minimum load increases as M increases.

Note that another consequence of the circular geometry is that for values of $\epsilon > \pi/2$ (all in the super-critical regime) the sign of the resultant P cannot be used to ascertain the nature of the pressure traction. For instance, at $\delta = 0$ and $M = 1$ in Fig. 5c, corresponding to a contact half-angle $\epsilon = 2.41$ radians, the transmitted pressure traction is highly tensile, but the resultant force P is positive (downward). This is because when the arc of contact is much larger than $\pi/2$, tensile adhesive tractions near the edges of contact have a downward component that opposes the resolved upward component of tensile adhesive forces near the center ($\phi = 0$). When the contact angle is smaller (in the sub-critical regime), the contribution of the traction to the resultant P has the same sign throughout the contact in a manner similar to halfspace adhesive contacts. For instance, only negative resultants P occur when the approach $\delta = 0$ in Fig. 3b.

While this is one possible geometric explanation stemming directly from the requirement that the adhesion always induce a tensile singularity at the edge of contact, the lack of equilibrium noted earlier may be established definitely only once other possible contact configurations (e.g. two separate contacts) are ruled out. Another possible explanation is that JKR-type models ignore the effect of adhesive forces outside the contact. Whether or not this is the cause may only be ascertained by considering models that include such behavior (e.g. the self-consistent model). It is,

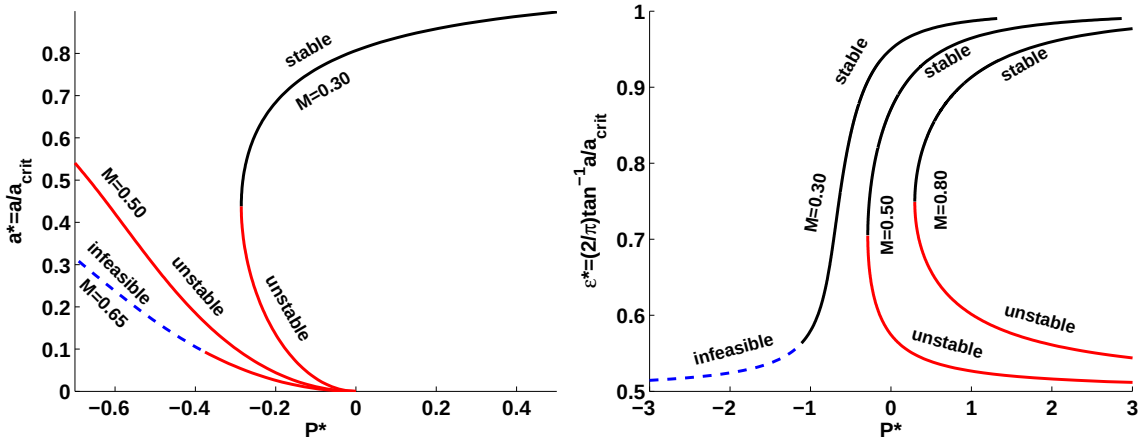

Fig. 11. Fixed-load stability of cylindrical contact equilibria in the (a) sub-critical and (b) super-critical regimes at the indicated values of adhesion parameter M. $\vartheta = 1.0$.

however, clear that these effects are not present at low M and even moderately large contact angles. Further, for the special case of a rubbery cylinder (section 7.2) there are no such anomalies at any value of M. Thus, the model is perfectly suited as an improvement to the Barquins half-plane solution in these parametric regimes.

8.3 Fixed-load stability

The regimes of stability of the equilibria described in the preceding sections will be examined more closely here. Figs. 11a and 11b depict fixed-load stability behavior in the sub- and super-critical regimes. The values of the adhesion parameter, M, are chosen to be representative. Fixed-load stability is ascertained numerically by examining the sign of the derivative $\partial G/\partial a|_P$. It is seen (Fig. 11a) that subcritical, low-adhesion stability behavior (M=0.30) is qualitatively most similar to classical JKR-adhesive behavior, with similar stable and unstable branches indicating JKR-type 'snap-in'. At a higher value such as M=0.50, the minimum in the a^*/P^* curve disappears, and fixed-load equilibria are unstable everywhere in the subcritical regime. In the supercritical regime, however, stable equilibria exist for these larger values of M. There is also a corresponding unstable branch at smaller contact angles, as Fig. 11b shows. Note that detachment by an applied upward load occurs at $M = 0.50$ (since the minimum is at $P^* < 0$), but does not occur on increasing M even further to 0.80, where overclosures with the confining body precedes detachment. In both plots, infeasible equilibria that violate the gap inequality are indicated by dashed lines. Nothing may be said about stability in these regimes without examining the two contact equilibrium. Note that at $M = 0.3$, there are stable super-critical contact states in addition to the stable sub-critical contact states.

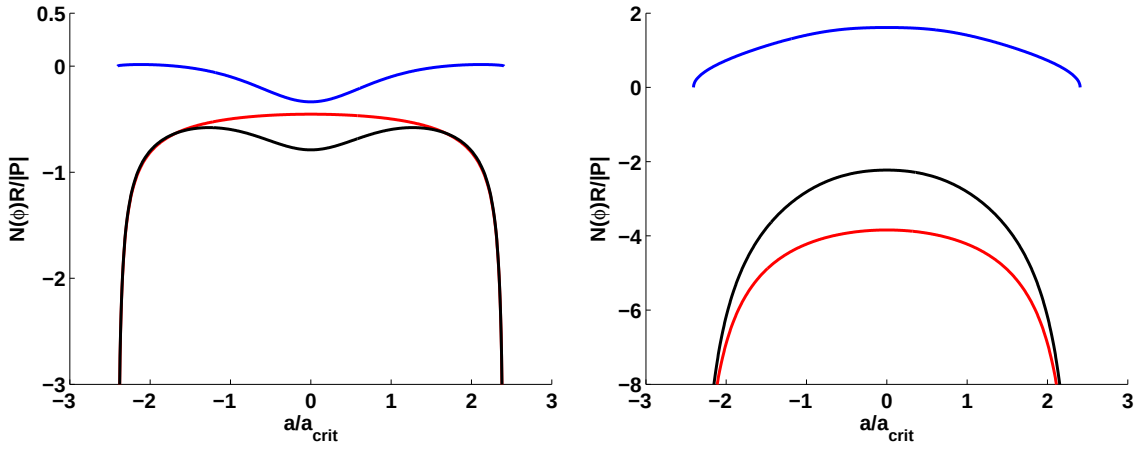

(a) (b)

Fig. 12. Bounded, unbounded and total normalized contact pressure $N(\phi)R/|P|$ at $M = 0.4, P^* = -0.46$ (a) and $M = 0.6, P^* = -0.08$ (a) in the super-critical region $a > a_{crit}$. $\vartheta = 1.0$. The bounded component does not correspond to the solution of an adhesionless contact problem in either case.

8.4 On the method of superposition and the gap inequality

Consider the pressure tractions at two different super-critical equilibrium states shown in Fig. 12. An important observation is that in neither case does the bounded component correspond to the solution of an adhesionless ($M = 0$) contact problem. This is because of the violation of the pressure inequality by the bounded component in plot 12a and violation of the gap inequality by this component in plot 12b. In fact, these bounded pressure states may not be reached under adhesionless contact conditions even on applying an infinite load. The components of the pressure, while being bounded and unbounded as expected, do not correspond to the solution of any individual contact / punch problems as is usual in JKR superposition. This is not altogether surprising, considering the nonlinearity of the contact boundary conditions: In general, no process other than enforcement of the contact boundary conditions will lead to the solution, and in so doing, the final pressure solution will satisfy the contact boundary conditions even when one its components may not (or even, as in the present case, represent the solution to *any* contact problem).

The importance of the gap inequality for the cylindrical system has already been demonstrated in this work, but it is by no means limited to such contacts. It suffices to say that in any contact system where exterior overclosures are likely, e.g. any indenter with concavities, it is advisable to test that the gap inequality is not violated by the proposed adhesive contact solution.

Conclusions

Planar JKR adhesive solutions using the half-plane assumption do not permit calculation of the approach or visualization of adhesive force-displacement curves unless the contact is periodic. By considering a conforming cylindrical contact and using an arc crack analogy, the approach and load-contact size relations to a planar adhesive problem were obtained in closed-form. The contact pressure distribution was also obtained in closed-form. The solutions reduce to known cases in both the adhesion-free and small-contact (Barquins) limits. The cylindrical system shows two distinct regimes of adhesive behavior; in particular, contact sizes exceeding the critical (maximum) size seen in adhesionless contacts are possible. The adhesion and detachment of a rubbery cylinder from a rigid cradle is qualitatively most similar to classical JKR contacts. A comparison of the cylindrical solution with the half-plane adhesive solution indicates that the latter typically underestimates the adherence force. The existence of stable, supercritical contact states is a novel feature of the adhesive cylindrical system.

Appendix

Consider the CPV

$$I_1(x) = \fint_{-a}^{a} \frac{\sqrt{a^2 - s^2}}{x - s} \tan^{-1}(s) ds \quad -a < x < a \tag{A.1}$$

This integral is difficult to evaluate by standard methods. However, $I_1(x)$ may be converted into the following double-integral

$$I_1(x) = \fint_{-a}^{a} \frac{\sqrt{a^2 - s^2}}{x - s} \left(s \int_0^1 \frac{dr}{1 + s^2 r^2} \right) ds \tag{A.2}$$

Since only one of the integrals is singular, it is possible to change the order of integration

$$I_1(x) = \int_0^1 \left(\fint_{-a}^{a} \frac{\sqrt{a^2 - s^2}}{x - s} \frac{s}{1 + s^2 r^2} ds \right) dr \tag{A.3}$$

The inner integrand may be separated using partial fractions and evaluated using $\fint_{-a}^{a} \frac{\sqrt{a^2-s^2}ds}{x-s} = \pi x$

$$\frac{1}{\pi} I_1(x) = \int_0^1 \frac{x^2}{1 + x^2 r^2} dr - \int_0^1 \frac{\sqrt{1 + a^2 r^2} - 1}{r^2 (1 + x^2 r^2)} dr \tag{A.4}$$

Again, expanding the second integral using partial fractions and integrating, one is left with an elementary result

$$I_1(x) = \pi \left[\sqrt{1+a^2} - 1 - \frac{\sqrt{a^2-x^2}}{2} \log \left\{ \frac{\sqrt{1+a^2}+\sqrt{a^2-x^2}}{\sqrt{1+a^2}-\sqrt{a^2-x^2}} \right\} \right] \tag{A.5}$$

The integral $I_2(x)$ may be evaluated using elementary methods.

$$I_2(x) = \int\!\!\!\!\!\!-_{-a}^{a} \frac{s\sqrt{a^2-s^2}}{(x-s)(1+s^2)} ds = \frac{\pi x^2 - \pi(\sqrt{1+a^2}-1)}{1+x^2} \tag{A.6}$$

The following standard integrals are stated without proof

$$\int_{-a}^{a} \log \left(\frac{\sqrt{1+a^2}+\sqrt{a^2-x^2}}{\sqrt{1+a^2}-\sqrt{a^2-x^2}} \right) \frac{dx}{1+x^2} = \pi \log(1+a^2) \tag{A.7}$$

$$\int_{-a}^{a} \log \left(\frac{\sqrt{1+a^2}+\sqrt{a^2-x^2}}{\sqrt{1+a^2}-\sqrt{a^2-x^2}} \right) \frac{1-x^2}{(1+x^2)^2} dx = \pi \frac{a^2}{1+a^2} \tag{A.8}$$

$$\int_{-a}^{a} \frac{1}{\sqrt{a^2-x^2}} \frac{dx}{1+x^2} = \frac{\pi}{\sqrt{1+a^2}} \tag{A.9}$$

$$\int_{-a}^{a} \frac{\sqrt{a^2-x^2}}{(1+x^2)^2} dx = \frac{\pi a^2}{2\sqrt{1+a^2}} \tag{A.10}$$

$$\int_{-a}^{a} \frac{1}{\sqrt{a^2-x^2}} \frac{1-x^2}{(1+x^2)^2} dx = \frac{\pi}{(1+a^2)^{3/2}} \tag{A.11}$$

$$\int_{-a}^{a} \sqrt{a^2-x^2} \frac{1-x^2}{(1+x^2)^3} dx = \frac{\pi a^2(2+a^2)}{4(1+a^2)^{3/2}} \tag{A.12}$$

It may be noted that $\tanh^{-1}(z) = \frac{1}{2}\log\left(\frac{1+z}{1-z}\right)$ by definition.

The sum of the infinite series of integrals required to calculate the approach in Eq. (5.7) are obtained as follows. Two are given in Noble and Hussain (1969) and may be used directly

$$\sum_{n=2}^{\infty} \frac{n}{n^2-1} \int_0^{\epsilon} \cos(n\psi)\cos(\psi/2)\sqrt{\cos^2(\psi/2)-\cos^2(\epsilon/2)}d\psi = \frac{\pi}{16}\left[\log\sin(\epsilon/2)\left(-3+2\cos\epsilon+\cos^2\epsilon\right) - \frac{1}{2} + \frac{1}{2}\cos^2\epsilon\right] \tag{A.13}$$

$$\sum_{n=2}^{\infty} \frac{n}{n^2-1} \int_0^{\epsilon} \cos(n\psi) \log \left(\frac{\cos(\psi/2) + \sqrt{\cos^2(\psi/2) - \cos^2(\epsilon/2)}}{\cos(\epsilon/2)} \right) d\psi = \frac{\pi}{8} \left[\log \sin(\epsilon/2) \left(-2 + 2\cos\epsilon\right) - \frac{1}{2} + \frac{1}{2}\cos\epsilon \right] \quad \text{(A.14)}$$

In addition, one requires the following result for the infinite sum of integrals involving unbounded integrands

$$\sum_{n=2}^{\infty} \frac{n}{n^2-1} \int_0^{\epsilon} \frac{\cos(n\psi)\cos(\psi/2)}{\sqrt{\cos^2(\psi/2) - \cos^2(\epsilon/2)}} d\psi = -\frac{\pi}{4} \cos^2(\epsilon/2) \left[3 + 4 \log \sin(\epsilon/2)\right] \quad \text{(A.15)}$$

This result may be derived by differentiating both sides of Eq. (A.13) with respect to ϵ using the Leibniz formula for differentiation under the integral sign, and simplifying.

Acknowledgement

This work was supported by NSF Grants CMMI 0928337 and CMMI 1031056.

References

Barber, J.R., 2010. Elasticity. Solid Mechanics and its Applications, Vol. 172. Springer Science, 2010.

Barquins, M., 1988. Adherence and rolling kinetics of a rigid cylinder in contact with a natural rubber surface. Journal of Adhesion, 26(1):1-12.

Carbone, G. and Mangialardi, L., 2004. Adhesion and friction of an elastic half-space in contact with a slightly wavy rigid surface. Journal of the Mechanics and Physics of Solids. 52(2004):1267–1287.

Carbone, G. and Mangialardi, L., 2008. Analysis of adhesive contact of confined layers by using a Greens function approach. Journal of the Mechanics and Physics of Solids, 56 (2):684- 706.

Chaudhary, M.K. and Weaver, T., 1996. Adhesive contact of cylindrical lens and a flat sheet. Journal of Applied Physics, 80(1):30–37.

Ciavarella, M. and Decuzzi, P. 2001. The state of stress induced by the plane frictionless cylindrical contact. I. The case of elastic similarity. International Journal of Solids and Structures, 38(2001):4507–4523.

Estrada, R. and Kanwal, R.P., 2000. Singular Integral Equations. Birkhauser, Boston.

Gladwell, G.M.L., 1980. Contact Problems in The Classical Theory of Elasticity. Monographs and Textbooks on Mechanics of Solids and Fluids. Sijthoff and Noordhoff, The Netherlands.

Guduru, P.R., 2007. Detachment of a rigid solid from an elastic wavy surface: Theory. Journal of the Mechanics and Physics of Solids, 55(2007):445–472.

Haiat, G. Phan Huy, M.C., and Barthel,E., 2003. The adhesive contact of viscoelastic spheres. Journal of the Mechanics and Physics of Solids. 51(2003):69–93.

Johnson, K.L., 1958. A note on the adhesion of elastic solids. British Journal of Applied Physics, 9(1):199–200.

Johnson, K.L. Kendall, K. and Roberts, A.D., 1971. Surface energy and the contact of elastic solids. Proceedings of the Royal Society of London. Series A, Mathematical and Physical Sciences, 324(1558):301–313

Johnson, K.L., 1995. The adhesion of two elastic bodies with slightly wavy surfaces. International Journal of Solids and Structures, 32(1995):423–430.

Kendall, K., Kendall, M. and Rehnfeldt, F. Adhesion of cells, viruses and nanoparticles. Springer Science, 2011.

Maugis, D. and Barquins, M. 1978. Fracture mechanics and the adherence of viscoelastic bodies. Journal of Physics D: Applied Physics, 11(1978):1989–2023.

Maugis, D., 2000. Contact, Adhesion and Rupture of Elastic Solids. First Edition. Springer Series in Solid-State Sciences. Vol. 130. Springer-Verlag Heidelberg 2000.

Noble, B. and Hussain, M.A., 1969. Exact solution of certain dual-series for indentation and inclusion problems. International Journal of Engineering Science, 7(11):1149–1161.

Spolenak, R. Gorb, S. Gao, H. and Arzt, E., 2005. Effects of contact shape on the scaling of biological attachments. Proceedings of the Royal Society A, 461(2005):305–319.

Sundaram, N. and Farris, T.N., 2010. Mechanics of advancing pin-loaded contacts with friction. Journal of the Mechanics and Physics of Solids, 58(2010):1819–1833.